Stable Vortex–Bright-Soliton Structures in Two-Component Bose-Einstein Condensates

K. J. H. Law,[1] P. G. Kevrekidis,[2] and Laurette S. Tuckerman[3]

[1]*Warwick Mathematics Institute, University of Warwick, Coventry CV4 7AL, United Kingdom*
[2]*Department of Mathematics and Statistics, University of Massachusetts, Amherst Massachusetts 01003-4515, USA*
[3]*PMMH-ESPCI, CNRS (UMR 7636), Université Paris 6 & 7, 75231 Paris Cedex 5, France*

(Received 26 January 2010; published 15 October 2010)

We report the numerical realization of robust two-component structures in 2D and 3D Bose-Einstein condensates with nontrivial topological charge in one component. We identify a stable symbiotic state in which a higher-dimensional bright soliton exists even in a homogeneous setting with defocusing interactions, due to the effective potential created by a stable vortex in the other component. The resulting vortex–bright-solitons, generalizations of the recently experimentally observed dark-bright solitons, are found to be very robust both in the homogeneous medium and in the presence of external confinement.

DOI: 10.1103/PhysRevLett.105.160405 PACS numbers: 03.75.Lm, 03.75.Mn, 03.75.Hh

Introduction.—Vortices in nonlinear field theory have a time-honored history [1]. They are among the most striking features of superfluids, play a role in critical current densities and resistances of type-II superconductors through their transport properties, and are associated with quantum turbulence in superfluid helium [2]. The advent of Bose-Einstein condensates (BECs) 15 years ago [3,4] has produced an ideal setting for exploring relevant phenomena. Since the experimental observation of matter-wave vortices [5], by using a phase-imprinting method between two hyperfine spin states of a ^{87}Rb BEC [6], the road opened for an extensive examination of vortex formation, dynamics, and interactions. Stirring the BECs [7] above a certain critical angular speed [8–11] led to the production of a few vortices [11] and even of very robust vortex lattices [12]. These structures have been produced by other experimental techniques, such as dragging obstacles through the BEC [13] or the nonlinear interference of condensate fragments [14]. Later, not only unit-charged but also higher-charged structures were produced [15] and their dynamical (in)stability was examined. This field also has strong similarities and overlap with the emergence of vortices and even vortex lattices in nonlinear optical settings; see, e.g., [16,17].

Another remarkable possibility in both BECs [18–20] and in nonlinear optics, e.g., [21], is that of multicomponent settings. Matter waves exhibit rich phase separation dynamics driven by the nonlinear interatomic interactions between different species or states that make up the BECs. Longitudinal spin waves [22], transitions between triangular and interlaced square vortex lattices [23], striated magnetic domains [24,25], and robust target patterns [26] have all been observed, as well as tunable interspecies interactions [27] and transitions between miscible and immiscible dynamics [28].

We interweave these two settings, motivated by Ref. [29] in which dark-bright solitons have been created in a quasi-1D two-component BEC, also per the original relevant suggestion of Ref. [30]. These are often termed "symbiotic solitons," as the bright component would be impossible to sustain under repulsive interatomic interactions (i.e., defocusing nonlinearities, as considered here), unless the dark component creates an "effective potential," of which the bright soliton is a bound state. The coupled bright solitary waves [31] and the gap ones of Ref. [32] constitute additional examples of symbiotic structures. We consider higher-dimensional realizations [30], i.e., vortex–bright-soliton states of various topological charge in 2D as well as in 3D [33]. We find these symbiotic configurations to be robust, with or without parabolic external confinement. In an optical lattice, the unstable vortex may in fact be stabilized by the bright soliton. The stability persists in 3D, while for traps elongated in the direction of the vortex core, additional negative energy (potentially instability-bearing) modes [34] emerge, as in the single-component vortex [35]. The work of Ref. [5] has already offered a prototypical dynamical realization of such states (analogous to their quasi-1D counterparts of Ref. [30] by Ref. [29]) and attests to their experimental relevance.

Physical setup.—The nondimensional Hamiltonian for a two-component condensate in the mean-field approximation reads [36]

$$H = \int d\mathbf{r}(\boldsymbol{\nabla}\Psi)^\dagger(\boldsymbol{\nabla}\Psi) + \Psi^\dagger V(\mathbf{r})\Psi + \frac{1}{2}|\Psi|^{2\dagger}U|\Psi|^2 - \Psi^\dagger M\Psi, \quad (1)$$

where $\Psi(\mathbf{r}) \in \mathbb{C}^2$ is the pseudospinor order parameter, $|\Psi|^2 = (|\Psi_1|^2, |\Psi_2|^2)^\dagger$, and $M = \mathrm{diag}\{\mu_1, \mu_2\}$ is the diagonal matrix of chemical potentials associated with the conservation of the number of atoms $N_1 = \int d\mathbf{r}|\Psi_1|^2$ and $N_2 = \int d\mathbf{r}|\Psi_2|^2$; a related useful diagnostic is $R = N_1/(N_1 + N_2) = N_1/N$. U is a 2×2 matrix accounting for the effectively nonlinear interatomic interactions. For the $|1, -1\rangle$ and $|2, 1\rangle$ components of ^{87}Rb, we can use [26] $U_{11} = 1.03$, $U_{12} = U_{21} = 1$, and $U_{22} = 0.97$. These

determine, through the negative sign of $\det(U) = |U|$, the immiscible nature of the interactions leading to phase separation [19,26]. The dimensional confining potential is

$$V(\mathbf{r}, z) = \underbrace{\frac{\omega_r^2}{4}|\mathbf{r}|^2 + \frac{\omega_z^2}{4}z^2}_{V_{\mathrm{MT}}} + \underbrace{A[\sin^2(2\omega_r x) + \sin^2(2\omega_r y)]}_{V_{\mathrm{OL}}}, \quad (2)$$

where V_{MT} is the parabolic component (often created magnetically) and V_{OL} the periodic (optical) lattice component. The time and length scales are $1/\omega_n$ and $\sqrt{\hbar/m\omega_n}$, respectively, where m is the atomic mass and ω_n is an arbitrary frequency in hertz. For ^{87}Rb with a scattering length of $a_{12} = 5.5$ nm, $(\omega_r, \omega_z) = 2\pi \times (8, 40)$ Hz, and by choosing $\omega_n = 5/4\omega_z$, the ratio between the actual and nondimensional number of atoms is $N_{\mathrm{fac,3D}} = (\hbar/2m\omega_n)^{3/2}(\hbar\omega_n/g_{3\mathrm{D}}) = 10$, where $g_{3\mathrm{D}} = (4\pi\hbar^2 a_{12}/m)$ is the dimensional interaction parameter. For a 2D reduction, the interaction parameter is $g_{2\mathrm{D}} = g_{3\mathrm{D}}(m\omega_z/2\pi\hbar)^{1/2}$ (e.g., [37]), and by taking $\omega_n = \omega_r$, the amplification factor is $N_{\mathrm{fac,2D}} = 30$. The equations of motion $(\dot{\Psi}, \text{c.c.})^T = J\sigma(\delta H/\delta\Psi, \text{c.c.})^T = J\sigma DH$, where $J = \mathrm{diag}(-iI, iI)$ and σ interchanges rows (3,4) with (1,2), for this infinite-dimensional Hamiltonian system are

$$i\dot{\Psi} = -\nabla^2\Psi + V(\mathbf{r})\Psi + U|\Psi|^2\Psi - M\Psi. \quad (3)$$

The stability of stationary solutions is determined by the eigenvalues of the Hessian of the Hamiltonian, $\sigma D^2 H$, and of $J\sigma D^2 H$. The linear stability is examined through the eigenvalues λ of the latter, with instability arising when $\mathrm{Re}(\lambda) \neq 0$. A linearly stable solution may become unstable if its linearization has eigenmodes with a negative projection onto the Hessian. Non-negativity of the Hessian precludes this and is an indication of *energetic stability*.

The variation can be posed in the $\{\Psi, \Psi^*\}$ or the $\{\Psi_{\mathrm{real}}, \Psi_{\mathrm{imag}}\}$ basis. The former is useful when the potential is axisymmetric, since then small excitations to a stationary solution $\Psi = (\Psi_1(r)e^{iS_1\theta}, \Psi_2(r)e^{iS_2\theta})$ of the form $\psi = (a_1, a_2)^T(\mathbf{r})e^{\lambda t} + (b_1, b_2)^T(\mathbf{r})e^{\lambda^* t}$ will have definite angular momentum $\alpha_j(r, \theta) = \tilde{\alpha}_j(r)e^{i\kappa_{\alpha_j}\theta}$. If we set $\kappa_{a_1} = \kappa$, then $\kappa_{b_1} = \kappa - 2S_1$, $\kappa_{a_2} = \kappa - S_1 + S_2$, and $\kappa_{b_2} = \kappa - S_1 - S_2$, so a single index κ will indicate the angular momentum of the excitation with given eigenvalue λ. Hence, the spectrum of eigenvalues $\{\lambda\}$ can be decomposed as the union of the spectra $\{\lambda_\kappa\}$ pertaining to angular momentum κ. We will also assume $S_2 = 0$, so that $S_1 = S$ and $\kappa_{a_2} = \kappa_{b_2}$. It has been shown numerically [34] and analytically [38] that instability windows arise in a single component with topological charge S only for wave numbers with $|\kappa| < S$. The null eigenvalues corresponding to gauge invariance appear in the spectrum of $\kappa = S$. For a single component in a parabolic trap, an anomalous mode for $\kappa = S - 1$ converges to zero as $\omega_r \to 0$, accounting for translational invariance and leading to the energetic stability of the $S = 1$ vortex without an external potential. For each $0 \leq \kappa < S - 1$ $(S > 1)$ an anomalous mode leads to windows of instability [34,38]. We show that these can be significantly suppressed, although the $S - 1$ spectrum occasionally leads to small instability windows for a small fraction bright-soliton component $N_2 \ll N_1$ for large N with a parabolic trap (no windows were observed without the trap).

Numerical methods.—Our methods extend those in, e.g., Refs. [39,40]. The spatial discretization in (r, θ, z) employs Chebyshev polynomials to represent r dependence [41]. The Fourier modes representing θ and z make the Laplacian operators diagonal in these directions. To identify stationary states of (3), we first obtain an initial estimate via imaginary-time (i.e., replacing $t \to it$) integration by using a first-order mixed implicit-explicit Euler scheme with $\Delta t = 10^{-2}$. We then refine the solution by using Newton's method. The linear system arising at each Newton step is solved by using the matrix-free induced dimension reduction [IDR(s)] algorithm [42,43], which requires only the action of the Hessian. To accelerate inversion, we precondition the system with the inverse Laplacian, by using its block diagonal structure. Hence, we solve the system $\nabla^{-2}D^2H(\Psi_n)\Delta_n = \nabla^{-2}DH(\Psi_n)$ and update $\Psi_{n+1} = \Psi_n - \Delta_n$ for $n = 0, 1, \ldots$. Fewer than 5 Newton iterations usually achieve an accuracy of $\|\nabla^{-2}DH(\Psi)\|_{l^2}/\|\Psi\|_{l^2} < 10^{-12}$.

For each stationary solution Ψ, we use the matrix-free implicitly restarted Arnoldi algorithm to iteratively compute the eigenpairs of the linearization $J\sigma D^2 H(\Psi)$ to a specified tolerance [44]. In order to find the desired eigenvalues we use inverse iteration, with the IDR(s) method and inverse Laplacian preconditioning to solve the linear systems, as above. Here, the preconditioner is taken to be $[J\sigma(\nabla^2)]^{-1}$, so that each iteration solves $\nabla^{-2}D^2H(\Psi)v_{n+1} = -\nabla^{-2}\sigma J v_n$.

We used a resolution in (r, θ, z) of $40 \times 64 \times 80$ to represent nonaxisymmetric solutions and eigenvectors. For axisymmetric solutions, quantitative accuracy requires only 30 radial modes for $N < 1000$ but up to 200 modes for larger N. For eigenvectors, we use only $S + 1$ modes in θ (see the introduction) and identify quantitatively all expected invariant and negative directions and windows of instability from Ref. [34].

Results.—In 2D $(\omega_z \to \infty)$ for $\omega_r = A = 0$, we first demonstrate in Fig. 1 the existence of an *energetically stable* (and hence also dynamically stable) vortex–bright-soliton state. This is so for all of the R and N values that we have sampled. A similar state exists for vortices of higher topological charge S, as shown in Fig. 1 for $S \leq 5$. The logarithmic scale shows that the soliton is more localized for larger S. In this case, the negative energy modes [34] in the spectra associated to $0 \leq \kappa < S - 1$ may lead to dynamical instability from complex quartets of eigenvalues

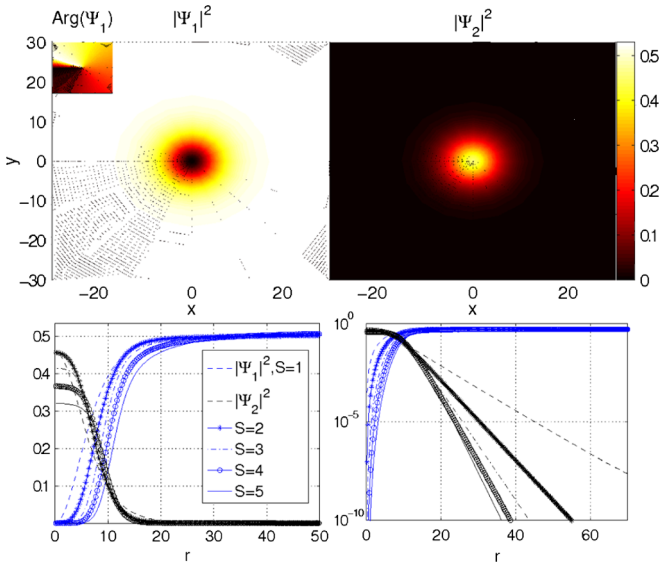

FIG. 1 (color online). The energetically stable $S = 1$ vortex-–bright-soliton without external potential for $R = 0.99$, $r_{\max} = 60$, and $N = 5900$ (top row). The bottom row shows radial profiles of unit and higher-charge vortex–bright-solitons in a homogeneous medium on a regular (left) and logarithmic (right) scale. All profiles are for $N = 10\,000$, $R = 0.99$, and $r_{\max} = 80$.

as a result of Hamiltonian-Hopf bifurcations which can occur upon collision with positive modes [45].

In a parabolic trap, the $S = 1$ vortex–bright-solitons remain dynamically stable. However, breaking of translational invariance produces a negative energy mode in the $\kappa = S - 1$ spectrum. Thus, an additional control parameter (through the atom number of the bright component) may lead to collisions of this mode with positive energy modes and, hence, rare isolated windows of instability arising for large $R < 1$ and large N; see Fig. 2 (left) for such a window for $S = 1$ as a function of R when $N = 4000$. A similar feature has recently been shown in the dark-bright 1D analog of the vortex–bright-soliton states [46].

For higher-charge vortex–bright-solitons, the same situation holds for the $\kappa = S - 1$ spectrum, while for $R = 1$ windows of instability arise from the negative modes in the spectra of $0 \leq \kappa < S - 1$. As R decreases, however, these

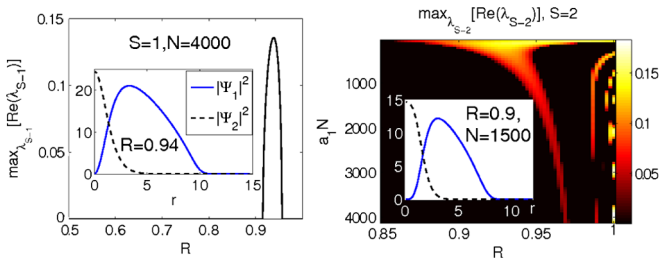

FIG. 2 (color online). Growth rate of the $S - 1$ mode as a function of R with $N = 4000$ for $S = 1$ (left) and growth rate of the $S - 2$ mode as a function of $R \times a_1 N$ for $S = 2$ (right).

windows of instability are generically suppressed by the increasing presence of the second bright component. Figure 2 (right) depicts the growth rate of the $S - 2$ spectrum for $S = 2$ over $R \times N$ parameter space. An example of the evolution of an unstable solution perturbed in the growing excitation direction is depicted in Fig. 3. The vortices first split from the center and begin to part and precess, but once they are far enough and the bright component is bimodal, they approach again and the bright component resumes unimodality. The sequence repeats, similarly to single-component $S = 2$ vortices [47].

When we impose an additional sinusoidal lattice potential $A > 0$, the one-component ($R = 1$) $S = 1$ vortex may become unstable (due to resonant eigenvalue collisions and ensuing oscillatory instabilities), at least for A sufficiently large [48]. The same holds for a large mass ratio $R < 1$. However, below a critical R, once again the bright component has a stabilizing influence.

The vortex–bright-soliton is stable in 3D without the trap and with periodic boundary conditions in z. Indeed, this is immediately clear upon Fourier transformation in z, since the spectrum of the Hessian decouples into an infinite family of subspectra equal to the 2D spectra shifted by k_z^2, and hence it remains non-negative. It is stable in the trapped case as well for $A = 0$ and $\omega_z = 5\omega_r$ and indeed for $\omega_z > \omega_r$. When $\omega_z = \omega_r$, the solution has another rotational invariance, and additional negative energy modes emerge for $\omega_z < \omega_r$. For $2\omega_z = \omega_r$ there are at least two additional negative energy modes, although this may not lead to dynamical instability. Upon addition of the lattice $A > 0$, the results are expected to be similar to 2D (up to considerations of the aspect ratio of the harmonic trapping). See Fig. 4 for an example with $\omega_z = 5\omega_r$.

Discussion.—We have illustrated the vortex–bright-soliton as a robust dynamical entity that emerges as a stable

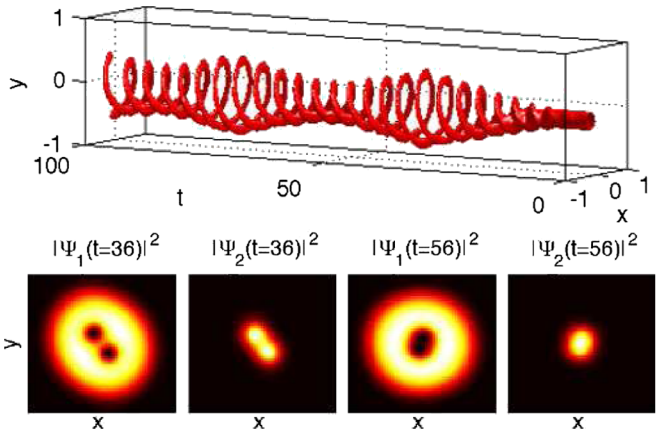

FIG. 3 (color online). The evolution in time of the unstable $S = 2$ solution for $(R, N) = (0.93, 200)$ perturbed in the direction of the growing excitation. Top: Approximate vorticity density isocontours show trajectories of the two vortices. Bottom: First splitting and rejoining.

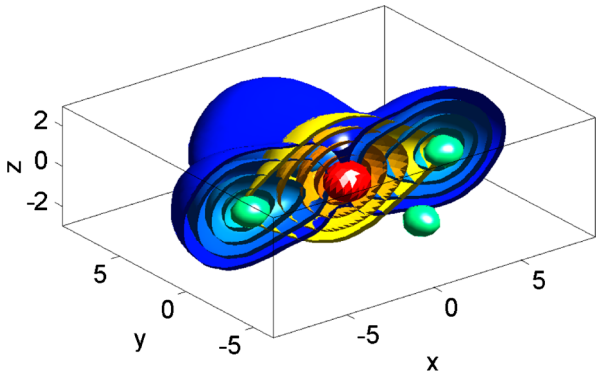

FIG. 4 (color online). Isocontours of the density of the stable symbiotic vortex–bright-solitons in the presence of an optical lattice with $\omega_z = 5\omega_r$, $R = 0.5$, and $N = 40$. Vortex surfaces are blue scale (darker) and soliton surfaces are yellow scale (lighter). This 3D stationary state is stabilized by the second component, which displaces the vortex component at its core.

structure in both 2D and 3D condensates (although similar concepts could be directly applicable to the nonlinear optics of defocusing optical media). We also examined relevant structures in the presence of parabolic (magnetic) and periodic (optical) trapping and found that they remain stable. While instabilities may arise (e.g., for higher topological charge S or as a result of the lattice), these are usually alleviated or suppressed by the presence of the second component in 2D and 3D.

It would be interesting to determine the robust existence of such waveforms, which are well within the reach of recent experiments, e.g., [26,28]. Our study suggests that higher-charge vortices in a single component may be stabilized by an external blue-detuned laser-beam potential acting as the bright soliton here. Hence, the stability of such vortices should be systematically examined in the presence of external potentials. Other themes such as multivortex–bright-soliton interactions and lattices would also be natural extensions of the present work.

P. G. K. acknowledges support from NSF and the Alexander von Humboldt Foundation.

[1] L. M. Pismen, *Vortices in Nonlinear Fields* (Oxford Science, Oxford, 1999).
[2] R. J. Donnelly, *Quantized Vortices in Helium II* (Cambridge University Press, Cambridge, England, 1991); D. R. Tilley and J. Tilley, *Superfluidity and Superconductivity* (IOP, Philadelphia, 1990).
[3] M. H. Anderson *et al.*, Science **269**, 198 (1995).
[4] K. B. Davis *et al.*, Phys. Rev. Lett. **75**, 3969 (1995).
[5] M. R. Matthews *et al.*, Phys. Rev. Lett. **83**, 2498 (1999).
[6] J. E. Williams and M. J. Holland, Nature (London) **401**, 568 (1999).
[7] K. W. Madison *et al.*, Phys. Rev. Lett. **84**, 806 (2000).
[8] A. Recati, F. Zambelli, and S. Stringari, Phys. Rev. Lett. **86**, 377 (2001).
[9] S. Sinha and Y. Castin, Phys. Rev. Lett. **87**, 190402 (2001).
[10] I. Corro, R. G. Scott, and A. M. Martin, Phys. Rev. A **80**, 033609 (2009).
[11] K. W. Madison *et al.*, Phys. Rev. Lett. **86**, 4443 (2001).
[12] C. Raman *et al.*, Phys. Rev. Lett. **87**, 210402 (2001).
[13] R. Onofrio *et al.*, Phys. Rev. Lett. **85**, 2228 (2000).
[14] D. R. Scherer *et al.*, Phys. Rev. Lett. **98**, 110402 (2007).
[15] A. E. Leanhardt *et al.*, Phys. Rev. Lett. **89**, 190403 (2002); Y. Shin *et al.*, Phys. Rev. Lett. **93**, 160406 (2004).
[16] Yu. S. Kivshar *et al.*, Opt. Commun. **152**, 198 (1998).
[17] A. Dreischuh *et al.*, J. Opt. Soc. Am. B **19**, 550 (2002).
[18] C. J. Myatt *et al.*, Phys. Rev. Lett. **78**, 586 (1997).
[19] D. S. Hall *et al.*, Phys. Rev. Lett. **81**, 1539 (1998).
[20] D. M. Stamper-Kurn *et al.*, Phys. Rev. Lett. **80**, 2027 (1998).
[21] D. Rand *et al.*, Phys. Rev. Lett. **98**, 053902 (2007).
[22] H. J. Lewandowski *et al.*, Phys. Rev. Lett. **88**, 070403 (2002).
[23] V. Schweikhard *et al.*, Phys. Rev. Lett. **93**, 210403 (2004).
[24] H.-J. Miesner *et al.*, Phys. Rev. Lett. **82**, 2228 (1999).
[25] J. Stenger *et al.*, Nature (London) **396**, 345 (1998).
[26] K. M. Mertes *et al.*, Phys. Rev. Lett. **99**, 190402 (2007).
[27] G. Thalhammer *et al.*, Phys. Rev. Lett. **100**, 210402 (2008).
[28] S. B. Papp, J. M. Pino, and C. E. Wieman, Phys. Rev. Lett. **101**, 040402 (2008).
[29] C. Becker *et al.*, Nature Phys. **4**, 496 (2008).
[30] Th. Busch and J. R. Anglin, Phys. Rev. Lett. **87**, 010401 (2001).
[31] V. M. Pérez-García and J. B. Beitia, Phys. Rev. A **72**, 033620 (2005).
[32] S. K. Adhikari and B. A. Malomed, Phys. Rev. A **77**, 023607 (2008).
[33] We consider only repulsive interactions, where such structures are symbiotic. With an attractive interaction, where such states can be self-trapped with a vanishing tail, they were originally proposed in Z. H. Musslimani *et al.*, Phys. Rev. Lett. **84**, 1164 (2000).
[34] H. Pu *et al.*, Phys. Rev. A **59**, 1533 (1999).
[35] D. L. Feder *et al.*, Phys. Rev. Lett. **86**, 564 (2001).
[36] C. J. Pethick and H. Smith, *Bose-Einstein Condensation in Dilute Gases* (Cambridge University Press, Cambridge, England, 2002).
[37] W. Bao, D. Jaksch, and P. A. Markowich, J. Comput. Phys. **187**, 318 (2003).
[38] R. Kollár and R. L. Pego, report, http://www.math.cmu.edu/CNA/Publications/publications2009/017abs/017abs.html.
[39] C. Huepe *et al.*, Phys. Rev. A **68**, 023609 (2003).
[40] T. Kapitula, K. J. H. Law, P. G. Kevrekidis, SIAM J. Appl. Dyn. Syst. **9**, 34 (2010).
[41] L. N. Trefethen, *Spectral Methods in MATLAB* (SIAM, Philadelphia, 2000).
[42] Peter Sonneveld and Martin B. van Gijzen, SIAM J. Sci. Comput. **31**, 1035 (2008).
[43] http://ta.twi.tudelft.nl/NW/users/gijzen/IDR.html.
[44] http://www.caam.rice.edu/software/ARPACK/.
[45] J. C. van der Meer, Nonlinearity **3**, 1041 (1990).
[46] S. Middelkamp *et al.*, arXiv:1005.3789.
[47] H. M. Nilsen and E. Lundh, Phys. Rev. A **77**, 013604 (2008).
[48] K. J. H. Law *et al.*, Phys. Rev. A **77**, 053612 (2008).